Published in final edited form as:

Sci Signal. 2024 April 09; 17(831): eadg7867. doi:10.1126/scisignal.adg7867.

Miz1 represses type I interferon production and limits viral clearance during influenza A virus infection

Wenjiao Wu[1,2,3,†], **Vinothini Arunagiri**[1,†], **Hanh Chi Do-Umehara**[1], **Cong Chen**[4], **Shuyin Gu**[2], **Indrani Biswas**[1], **Karen M. Ridge**[4], **G. R. Scott Budinger**[4], **Shuwen Liu**[2,5,*], **Jing Liu**[1,*]

[1]Department of Surgery, College of Medicine; Cancer Center, University of Illinois at Chicago, Chicago, IL 60612, USA

[2]Guangdong Provincial Key Laboratory of New Drug Screening, School of Pharmaceutical Sciences, Southern Medical University, Guangzhou, China.

[3]Department of Pharmacy, Guangdong Second Provincial General Hospital, 466 Middle Xingang Road, Guangzhou, 510317, Guangdong, China.

[4]Division of Pulmonary and Critical Care Medicine, Feinberg School of Medicine, Northwestern University, Chicago, IL 60611, USA.

[5]State Key Laboratory of Organ Failure Research, Southern Medical University, Guangzhou 510515, China.

Abstract

Type I interferons (IFNs) are critical for the antiviral immune response, and finetuning type I IFN production is critical to effectively clearing viruses without causing harmful immunopathology. We showed that the transcription factor Miz1 epigenetically repressed the expression of genes encoding type I IFNs in mouse lung epithelial cells by recruiting histone deacetylase 1 (HDAC1) to the promoters of *Ifna* and *Ifnb*. Loss of function of Miz1 resulted in augmented production of these type I IFNs during influenza A virus (IAV) infection, leading to improved viral clearance in vitro and in vivo. IAV infection induced Miz1 accumulation by promoting the Cullin-4B (CUL4B)–mediated ubiquitylation and degradation of the E3 ubiquitin ligase Mule (Mcl-1 ubiquitin ligase E3; also known as Huwe1 or Arf-BP1), which targets Miz1 for degradation. As a result, Miz1 accumulation limited type I IFN production and favored viral replication. This study reveals a previously unrecognized function of Miz1 in regulating antiviral defense and a potential mechanism for influenza viruses to evade host immune defense.

[*]Corresponding author. jinglius@uic.edu (J.L.); liusw@smu.edu.cn (S.L.).
[†]These authors contributed equally to this work.

Author contributions: W.W., S.L., and J.L. designed the research. H.C.D., C.C., S.G., and I.B. performed the research and analyzed the data. K.M.R. and G.R.S.B. provided reagents. S.L. and J.L. supervised the study. W.W. wrote the manuscript. J.L. edited the manuscript. All authors have read and approved the manuscript.

Competing interests: The authors declare that they have no competing interests.

Data materials and availability: All data needed to evaluate the conclusions in the paper are present in the paper or the Supplementary Materials.

Introduction

Influenza viruses are important pathogens that cause mild to severe respiratory infections in humans and animals and are a major health problem (1). Influenza viruses are enveloped, negative-sense, single-stranded RNA viruses, and are categorized as the influenza A, B, C, and D viruses. Influenza A virus (IAV) is one of the most common pathogenic subtypes in humans, causing pneumonia-related respiratory disease and death (2–6) (7). The main target for the influenza virus is the epithelium of the host respiratory tract, which orchestrates the innate immune response and constitutes the first line of host defense against viral infection (3, 8, 9). Viral replication–induced viral DNA-RNA hybrids in lung epithelial cells are recognized as pathogen-associated molecular patterns (PAMPs) by host pattern-recognition receptors (PRRs), including retinoic acid–inducible gene I (RIG-I) and melanoma differentiation-associated protein 5 (MDA5) (10). Activated RIG-I and MDA5 in turn bind to mitochondrial antiviral signaling protein (MAVS), resulting in the recruitment of downstream signaling adaptors, which leads to the production of type I interferons (IFNs) and proinflammatory cytokines and chemokines. Type I IFNs stimulate the expression of hundreds of genes that are collectively known as IFN-stimulated genes (ISGs) in neighboring cells, which induces an antiviral state. On the other hand, proinflammatory cytokines and chemokines recruit additional immune cells and mediate viral clearance (10–13).

Type I IFNs, including IFN-α and IFN-β, are important for host defense against viruses (14, 15). Insufficient IFN production causes chronic infection; however, excessive IFN production causes immunopathology that can lead to autoimmune or inflammatory diseases (16, 17). Therefore, fine-tuning IFN production is critical for effective viral clearance without inducing harmful immunopathology (14, 16). The production of type I IFN is subject both transcriptional and posttranslational regulation (12). At the transcriptional level, IFN regulatory factor 3 (IRF3) and IRF7 are the fundamental transcription factors that induce the expression of genes encoding type I IFNs. These factors are activated through their phosphorylation by the kinases TANK-binding kinase 1 (TBK1) and inhibitor of κB (IκB) kinase-ε (IKKε) upon activation of the RIG-I/MDA5–MAVS pathway (12, 18, 19). Nuclear factor−κB (NF−κB) is also required as a cofactor to induce the expression of genes encoding type I IFN s (20–22). Viruses that develop efficient defense strategies to conquer host antiviral effectors will be successful in establishing infections. For example, viruses can inhibit type I IFN production and weaken innate antiviral immune responses (23, 24); however, the underlying molecular mechanisms remain incompletely understood.

Myc-interacting zinc finger protein 1 (Miz1; also known as Zbtb17) belongs to the poxvirus and zinc-finger (POZ) domain/zinc finger transcription factor family. It has an N-terminal POZ domain that is required for its transcriptional activity and 13 zinc fingers at its C terminus (25, 26). Miz1 preferentially binds at the initiation region of a gene and either activates gene transcription directly or represses gene transcription through its interactions with other regulatory factors, such as Myc, Myc-associated factor X (Max), and B-cell lymphoma 6 protein (BCL-6), serving critical roles in cell proliferation, differentiation, cell-cycle progression, and apoptosis (27–29). We previously reported that loss of function of Miz1 in mice augments the expression of genes encoding proinflammatory factors,

which results in worsened lung inflammation and injury in response to challenge with lipopolysaccharide (LPS), whereas it results in improved survival in response to live bacterial infection associated with increased bacterial clearance (30). Whether Miz1 plays a role in the antiviral immune response is unclear. Here, we showed that IAV infection resulted in the accumulation of Miz1 protein, which in turn repressed the production of type I IFNs and limited viral clearance.

Results

Miz1 inhibits type I IFN production and promotes viral replication during IAV infection of lung epithelial cells

The main target for influenza viruses is the respiratory epithelium, which orchestrates the innate immune response and constitutes the first line of host defense against viral infection (3, 8, 9). To investigate the possible involvement of Miz1 in regulating the immune response to IAV infection, we infected a stable murine type II-like lung epithelial cell line (MLE-12) (30), in which Miz1 was knocked down by short hairpin RNA (shRNA) (MLE-12/shMiz1; fig. S1A), with H1N1 A/WSN/1933 (WSN) viruses and analyzed *Ifn* expression by quantitative PCR (qPCR). WSN induced the expression of both *Ifnb1* (which encodes mouse IFN-β protein) and *Ifna1* (which encodes mouse IFN-α protein) in a time-dependent manner in the control MLE-12/shCtrl cells (Fig. 1, A and B). Increased amounts of *Ifna1* and *Ifnb1* mRNAs were observed in WSN-treated MLE-12/shMiz1 cells compared to those in WSN-infected control MLE-12/shCtrl cells at almost all times up to 24 hours after infection (Fig. 1, A and B).

Type I IFNs are potent inhibitors of viral replication. Accordingly, plaque assays performed with cell culture medium harvested at 24 hours after infection with WSN showed decreased viral titers in the medium from MLE-12/shMiz1 cells compared to that from control MLE-12/shCtrl cells (Fig. 1C). The amounts of *NP* mRNA, which encodes viral nucleoprotein (NP), a structural protein that encapsulates the negative-strand viral RNA, and *HA* mRNA, which encodes influenza hemagglutinin (HA), the antigenic glycoprotein on the surface of the virus, were increased in a time-dependent manner upon WSN infection of control MLE-12/shCtrl cells (fig. S1B), indicating active viral replication. The amounts of *NP* and *HA* mRNAs were substantially reduced in WSN-treated MLE-12/shMiz1 cells at all times up to 24 hours after infection (fig. S1B), indicating inhibition of viral replication. Furthermore, the expression of exogenous Miz1 decreased IFN-β production and rescued viral replication in MLE-12/shMiz1 cells, as indicated by the expression of NP (fig. S1, C and D).

To further validate these findings, we knocked out Miz1 in MLE-12 cells using the CRISPR/Cas 9 system (fig. S1E). Increased *Ifnb1* mRNA abundance was observed in WSN-infected MLE-12/Miz1 KO cells as compared to that in WSN-infected control wild-type (WT) cells at almost all times up to 24 hours after infection (Fig. 1D, left). This finding was supported by the increased amount of IFN-β detected in the culture medium from WSN-infected MLE-12/Miz1 KO cells as compared to that for WSN-infected control WT cells (Fig. 1D, right). In addition, at 24 hours after WSN infection, *Ifna1* mRNA abundance was markedly increased in MLE-12/Miz1 KO cells compared to that in control

cells (Fig. 1E). Consequently, decreased viral titers and reduced expression of *NP* and *HA* were observed in WSN-infected MLE-12/Miz1 KO cells as compared to control WT cells (Fig. 1F, fig. S1F). The expression of exogenous Miz1 in WSN-infected Miz1 KO cells led to a decrease in *Ifna1* and *Ifnb1* mRNA abundances (Fig. 1, G and H). Moreover, we investigated the role of Miz1 in the human lung epithelial cell lines BEAS-2B and A549 with a combination of three small interfering RNAs (siRNAs) to silence Miz1. Similar to the results from the experiments with murine cell lines, silencing of Miz1 in BEAS-2B and A549 cells resulted in increased *IFN* expression and decreased viral titers (fig. S1, G and H). Furthermore, BEAS-2B and A549 cells stably expressing Miz1-specific shRNA showed increased *IFN* expression (fig. S1, I and J). Together, these data suggest that Miz1 inhibits *Ifn* expression and facilitates viral replication during IAV infection.

The N-terminal POZ domain is required for Miz1-mediated transcriptional activity [19, 20]. To determine whether the effect of Miz1 on the regulation of *IFN* expression and viral replication depended on the POZ domain, we used stable MLE-12 cell lines generated previously (30), which express Miz1-specific shRNA and exogenous, shRNA-resistant WT Miz1 or the POZ domain deletion mutant of Miz1 [MLE12–Miz1(WT) or MLE-12–Miz1(ΔPOZ)] (fig. S1K). Similar to MLE-12/shMiz1 and MLE-12/Miz1 KO cells, MLE-12–Miz1(ΔPOZ) cells had increased IFN-I expression, decreased viral titers, and reduced NP protein abundance during WSN infection (Fig. 1, I to K, fig. S1L). These data suggest that Miz1 regulates the antiviral immune response in a POZ domain–dependent manner.

Miz1 inhibits the production of type I IFN in response to a double-stranded RNA analog in lung epithelial cells

Polyinosinic:polycytidylic acid [poly(I:C)] is a synthetic analog of double-stranded RNA (dsRNA), which is used in preclinical models to mimic the replication intermediates present in cells infected with RNA viruses, because most viruses produce dsRNA during their replication (31). Consistent with the results obtained from experiments with live WSN infection, poly(I:C) induced the increased expression of *IFN* and production of IFN-β in MLE-12/Miz1 KO and MLE-12–Miz1(ΔPOZ) cells compared to that in their corresponding controls (Fig. 2, A to D).

Mutation of Ser^{178} of Miz1 results in increased type I IFN production and improved viral clearance

We previously reported that the phosphorylation of Miz1 at Ser^{178} is important for its transcriptional regulatory function (30). To determine whether Ser^{178} phosphorylation was involved in Miz1 regulation of IFN-I during influenza virus infection, we used MLE-12/Miz1(WT) and MLE-12/Miz1(S178A) cells expressing Miz1-specific shRNA and exogenous, shRNA-resistant WT Miz1 or S178A mutant Miz1, in which Ser^{178} is mutated to the non-phosphorylatable alanine, as we previously reported (Fig. 3A) (30). We observed increased *Ifn* expression and decreased viral titers in WSN-treated MLE-12/Miz1(S178A) cells compared to those in WSN-treated MLE-12/Miz1(WT) cells (Fig. 3, B to D). Similarly, poly(I:C) induced increased *Ifnb1* expression in MLE-12/Miz1(S178A) cells compared to that in MLE-12/Miz1(WT) cells (Fig. 3E). *Ifna1* expression was also enhanced in MLE-12/

Miz1(S178A) cells compared to that in MLE-12/Miz1(WT) cells at 4 and 8 hours after poly(I:C) treatment (Fig. 3F). Together, these data suggest that Ser^{178} is required for Miz1 to inhibit type I IFN production and thereby suppress viral clearance during IAV infection.

Miz1 interferes with the binding of IRF3 and IRF7 to the *Ifnb1* promoter

The induction of type I IFN expression depends on the activation of IRF3 and IRF7, which are activated through phosphorylation by TBK1 and IKKε (12, 18, 19). Thus, we investigated whether Miz1 affected the phosphorylation and activation of IRF3 and IRF7. Western blotting analysis showed similar amounts of phosphorylated IRF3 and IRF7 in WSN-infected MLE12–Miz1(WT) and MLE-12–Miz1(ΔPOZ) cells (fig. S2, A and B). Additionally, we observed comparable nuclear translocation of IRF3 and IRF7 between WSN-infected MLE12–Miz1(WT) and MLE-12–Miz1(ΔPOZ) cells (fig. S2C). IAV infection also activates members of the mitogen-activated protein kinase (MAPK) family, including extracellular signal–regulated kinase (ERK), p38, and c-Jun N-terminal kinase (JNK), which contribute to type I IFN production (32–34). We found that there was no difference in the phosphorylation of these MAPKs between MLE12–Miz1(WT) and MLE-12–Miz1(ΔPOZ) cells (fig. S2A).

To determine whether Miz1 acted as a transcription factor to regulate the activity of the *Ifnb1* promoter, we transfected MLE12–Miz1(WT) and MLE-12–Miz1(ΔPOZ) cells with an *Ifnb1*-luciferase reporter construct (*Ifnb1*-promter driving luciferase) (35) together with a control *Renilla* reporter construct and then subjected the cells to WSN infection. WSN infection induced *Ifnb1*-luciferase activity in MLE12–Miz1(WT) cells at 24 hours, which was further increased in MLE-12–Miz1(ΔPOZ) cells under the same conditions (Fig. 4A). These data suggest that Miz1 represses *Ifnb1* promoter activity. To determine whether Miz1 repressed *Ifnb1* promoter activity by directly binding to the *Ifnb1* promoter, we performed chromatin immunoprecipitation (ChIP) assays with Miz1-specific antibody for immunoprecipitation (IP) in WSN-infected WT MLE-12 or MLE-12/Miz1 KO cells. WSN infection induced the recruitment of Miz1 to the *Ifnb1* promoter in WT MLE-12 cells but not in MLE-12/Miz1 KO cells (Fig. 4B). Consistently, WSN infection induced Miz1 recruitment to the *Ifnb1* promoter in MLE12–Miz1(WT) cells, which was inhibited in MLE-12–Miz1(ΔPOZ) cells (Fig. 4C). Miz1 binding to the *Ifnb1* promoter in response to WSN infection showed delayed kinetics compared to its rapid effect on *Ifnb1* mRNA synthesis (Fig. 1). This delay might be attributed to the sensitivity of ChIP detection, which may require greater Miz1 abundance for detectable binding. At early time points, reduced Miz1 abundance might promptly affect *IFN* mRNA synthesis but remain undetectable due to method sensitivity.

IRF3 and IRF7 are the fundamental transcription factors for the induction of genes encoding type I IFNs during influenza virus infection. We speculated that Miz1 might interfere with the binding of IRF3, IRF7, or both to the *Ifnb1* promoter, thereby repressing *Ifnb1* promoter activity. Indeed, IRF3 and IRF7 binding at the *Ifnb1* promoter was enhanced in MLE12–Miz1(ΔPOZ) cells compared to that in MLE12–Miz1(WT) cells at 6 and 12 hours after WSN infection (Fig. 4, D and E). In contrast, Miz1 did not affect the recruitment of the NF-κB subunit RelA to the *Ifnb1* promoter during IAV infection (fig. S2D), nor did it

interfere with the nuclear translocation of RelA in infected cells (fig. S2C). Furthermore, knocking down Miz1 enhanced the expression of *Il6* but not *Tnf*, both of which are NF-κB target genes, in response to WSN infection (fig. S2, E and F). These data suggest that Miz1 regulates specific gene expression through chromatin remodeling or epigenetic mechanisms, rather than having a general effect on NF-κB activation.

Miz1 recruits HDAC1 to the *Ifnb1* promoter

Posttranslational modification of histone lysine residues in chromatin plays an important role in the regulation of gene expression. Histone lysine acetylation results in chromatin decompaction and increased access of transcription factors to DNA and, thus, usually correlates with gene expression, whereas histone deacetylation renders nucleosomal DNA less accessible to the transcriptional machinery, thereby usually favoring transcriptional silencing (36–39). A previous report demonstrated that HDAC1, which catalyzes histone deacetylation, is a repressor of the *Ifnb1* promoter (40). Consistent with this report, we observed increased *Ifnb1* expression when HDAC1 was knocked down by siRNA during IAV infection (Fig. 5A). We previously reported that Miz1 exerts its epigenetic regulation by recruiting HDAC1 to a target promoter (30). We sought to determine whether Miz1 recruited HDAC1 to the *Ifnb1* promoter, resulting in histone deacetylation and thus reducing the binding of IRF3 and IRF7 to the *Ifnb1* promoter during IAV infection. ChIP assays showed that HDAC1 was recruited to the *Ifnb1* promoter after WSN infection in MLE12–Miz1(WT) cells, which was suppressed in MLE-12–Miz1(ΔPOZ) cells (Fig. 5B). Similar results were obtained with MLE-12/Miz1 KO cells as compared to control WT MLE-12 cells (Fig. 5C). Accordingly, histone acetylation (at Lys^9 and Lys^{14}) was increased in MLE-12–Miz1(ΔPOZ) cells as compared to that in MLE12–Miz1(WT) cells at 6 and 12 hours after WSN infection (Fig. 5D). These data suggest that Miz1 recruits HDAC1 to the *Ifnb1* promoter, resulting in histone deacetylation and inhibition of IRF3 and IRF7 binding. To investigate the mechanism by which Miz1 recruited HDAC1 to the *Ifnb1* promoter, we examined their potential interaction. Co-immunoprecipitation studies revealed an association between Miz1 and HDAC1 in MLE-12 cells under resting conditions (Fig. 5E), and WSN infection did not enhance this interaction (Fig. 5F). Note that the Miz1 POZ-domain deletion mutant maintained its interaction with HDAC1 (Fig. 5E), suggesting that this interaction is independent of the POZ domain. Together, these findings suggest that Miz1 associates with HDAC1 under resting conditions, and upon WSN infection, the Miz1-HDAC1 complex is recruited to the *Ifnb1* promoter to repress gene expression.

Loss of function of Miz1 enhances type I IFN production and improves survival in IAV-infected mice

To determine the role of Miz1 in regulating antiviral immune responses in vivo, we used $Miz1(POZ)^{fl/fl}$ mice, in which the exons encoding the Miz1 POZ domain are flanked by loxP sites (30). We previously reported that intratracheal administration of adenovirus encoding Cre recombinase (Ad-Cre) into $Miz1(POZ)^{fl/fl}$ mice results in deletion of the Miz1 POZ domain in the lungs ($Miz1^{\Delta POZ\text{-}lung}$ mice) (30). Here, $Miz1(POZ)^{fl/fl}$ mice were intratracheally instilled with Ad-Cre or the empty adenovirus vector (Ad-null). Thirty days later, mice were intratracheally infected with WSN. WSN infection resulted in 100% mortality within 10 days in the control, Ad-null-treated $Miz1(POZ)^{fl/fl}$ mice compared with

30% mortality after 14 days in the Miz1$^{\Delta POZ\text{-}lung}$ mice (Fig. 6A). In addition, Miz1$^{\Delta POZ\text{-}lung}$ mice lost weight upon WSN infection but began to regain weight from day 10 after infection, whereas the control mice lost weight continuously until death (Fig. 6B). We measured the kinetics of type I IFN induction upon WSN infection in wild-type C57BL/6 mice. *Ifnb1* and *Ifna1* expression was induced on days 3 and 5 after WSN infection, and on day 7, the abundances of *Ifnb1* and *Ifna1* mRNAs were not significantly different from those at baseline (fig. S3, A and B). Therefore, we chose day 4 after WSN infection to compare the induction of *Ifn* expression between the control and Miz1$^{\Delta POZ\text{-}lung}$ mice. The production of IFN-β in the bronchoalveolar lavage (BAL) fluid and the abundance of *Ifnb* mRNA in the lungs of Miz1$^{\Delta POZ\text{-}lung}$ mice were increased compared to those of the control mice on day 4 after infection (Fig. 6, C and D). There was also a trend of increased IFN-α production in the BAL fluid of Miz1$^{\Delta POZ\text{-}lung}$ mice (Fig. 6E). Accordingly, viral titers in the lungs were lower in Miz1$^{\Delta POZ\text{-}lung}$ mice than in control mice on day 4 after WSN infection (Fig. 6F). Together, these data suggest that loss of function of Miz1 increases *Ifn* expression during IAV infection, thereby inhibiting viral replication and improving survival in mice.

IAV infection reduces the abundance of the Miz1 E3 ubiquitin ligase Mule and induces Miz1 accumulation

We sought to determine whether and how Miz1 was regulated during IAV infection. MLE-12 cells were infected with WSN for different times, and we observed that Miz1 protein abundance was increased in a time-dependent manner (Fig. 7A), and the increase in Miz1 protein abundance correlated with increasing MOI (Fig. 7B). WSN infection also enhanced the nuclear translocation of Miz1 (fig. S4A). We did not observe a marked change in the abundance of *Zbtb17* mRNA (which encodes mouse Miz1 protein) within 24 hours after WSN infection (fig. S4B), which suggests posttranslational regulation of Miz1 by WSN infection. We previously reported that the E3 ubiquitin ligase Mule targets Miz1 for ubiquitination-dependent proteasomal degradation (41). We observed time- and dose-dependent decreases in Mule protein abundance in MLE-12 cells during WSN infection (Fig. 7, A and B). Similar results were obtained with poly(I:C) treatment: the time- and dose-dependent reduction in Mule protein abundance and a corresponding increase in the amount of Miz1 protein (Fig. 7, C and D). In WSN-infected mouse lungs, Miz1 protein abundance was also increased compared to that in uninfected lungs (Fig. 7E). In addition, *Zbtb17* mRNA abundance was unaltered in poly(I:C)-treated cells or WSN-infected mouse lungs (fig. S4, C and D). Together, these data suggest that IAV infection reduces Mule protein abundance, which might contribute to the accumulation of Miz1 protein. Supporting this notion, siRNA-mediated knockdown of Mule blocked the WSN-induced increase in *Ifnb1* mRNA abundance (Fig. 7F). We then investigated whether Mule acted through Miz1 to regulate the antiviral immune response. Consistent with our earlier findings, siRNA-mediated knockdown of Miz1 enhanced the WSN-induced increase in *Ifnb1* mRNA abundance (Fig. 7G). As expected, siRNA-mediated knockdown of Mule suppressed the WSN-induced increase in *Ifnb1* mRNA abundance (Fig. 7G). Furthermore, knockdown of Miz1 somewhat rescued the WSN-induced reduction in *Ifnb1* mRNA abundance caused by Mule knockdown (Fig. 7G). These data provide a causal link between Mule and Miz1 in regulating the antiviral response.

IAV infection induces increases the abundance of Cullin-4B (CUL4B), which targets Mule for ubiquitylation and degradation

We next investigated the mechanism by which IAV infection reduced the abundance of Mule. WSN infection did not markedly alter the abundance of *Huwe1* mRNA, which encodes mouse Mule (fig. S5A). Treatment with poly(I:C) did not alter *Huwe1* mRNA abundance at early time points (2 to 8 hours after treatment) (fig. S5B), when Mule protein abundance would be expected to be low based on earlier results (Fig. 7C). These data suggest that the WSN infection–induced reduction in Mule abundance occurs at a post-transcriptional level. We found that the proteasome inhibitor MG132, which was added after infection with WSN or treatment with poly(I:C), prevented the reduction in Mule protein abundance (Fig. 8, A and B), suggesting that IAV infection induces the proteasomal degradation of Mule. To determine whether Mule was degraded by the ubiquitin proteasome system, we cotransfected human embryonic kidney 293 (HEK-293) cells with plasmids encoding Flag (M2)-tagged Mule and HA-tagged ubiquitin, which was followed by WSN infection. Immunoprecipitation with an anti-Flag antibody in combination with Western blotting analysis with an anti-HA antibody showed that WSN infection resulted in Mule ubiquitylation (Fig. 8C). The cullin-E3 ligase family member CUL4B is an essential E3 ubiquitin ligase that targets Mule for ubiquitylation and degradation (42, 43). We found that WSN infection or poly(I:C) treatment increased the abundance of CUL4B protein, which correlated with a decrease in Mule abundance and the accumulation of Miz1 (Fig. 8, D and E). Co-immunoprecipitation assays showed that WSN infection induced an interaction between endogenous Mule and CUL4B (Fig. 8F), as well as an interaction between endogenous Mule and Miz1 (fig. S5C). Silencing CUL4B or treatment with MLN4924, a small-molecule inhibitor of CUL4B, inhibited the WSN-induced reduction in Mule abundance (Fig. 8, G and H). Accordingly, silencing of CUL4B resulted in a reduction in Miz1 protein abundance (Fig. 8I), which was accompanied by increased *Ifn* expression and enhanced viral clearance during WSN infection (Fig. 8, J and K). Similarly, MLN4924 also promoted viral clearance, as indicated by a decrease in viral NP abundance (Fig. 8L). Together, these data suggest that IAV infection induces the production of CUL4B, which targets Mule for ubiquitylation and degradation, resulting in the accumulation of Miz1, which represses type I IFN expression, thereby facilitating viral replication (Fig. 9).

Discussion

Influenza virus infections are a major public health problem, causing substantial morbidity and mortality worldwide (1, 6). Current anti-influenza therapies include yearly vaccinations and anti-viral drugs (6, 44); however, vaccines are not effective against novel pandemic strains due to antigenic drift and shift (45), and certain human populations are resistant to anti-viral drugs (6, 44). Targeting the host response against influenza virus is an alternative strategy that might be beneficial (6, 46). Type I IFNs, including IFN-α and IFN-β, are important for host defense against viruses, which inhibit viral replication and mediate the induction of antiviral adaptive immunity (14, 15). How type I IFNs are regulated during influenza virus infection remains incompletely understood. Here, we identified Miz1 as a transcriptional repressor of IFN-β production through epigenetic regulation during IAV infection and showed that it therefore regulates the antiviral immune response. We also

presented a mechanism of viral defense strategy through the accumulation of Miz1 through CUL4B-mediated degradation of the Miz1 E3 ligase, Mule.

Our data showed that during influenza virus infection, Miz1 recruited HDAC1 to the *Ifnb1* promoter, resulting in histone deacetylation, thereby reducing the accessibility of the *Ifnb1* promoter to IRF3 and IRF7. However, RelA binding to the *Ifnb1* promoter did not seem to be affected by Miz1. The binding of NF-κB to target promoters depends on the promoter context and on other coregulatory molecules (47, 48). Future studies will investigate the differential regulation of DNA accessibility to different transcription factors including IRF3, IRF7, and RelA by Miz1-mediated recruitment of HDAC1. One possibility is that whereas the IRF3 and IRF7 binding sites on the *Ifnb1* promoter are located close to the transcription start site (TSS) and Miz1 preferentially binds to the initiation region, multiple RelA binding sites span different regions of the *Ifnb1* promoter (20, 49). Therefore, there might be compensation for RelA binding from different locations on the *Ifnb1* promoter. Alternatively, the binding affinities of IRF3 and IRF7 as compared to that of RelA for DNA might be differentially regulated by the degree of local unwinding of nucleosomal DNA, which is controlled by the balance between histone acetylation and deacetylation (36–39).

We previously reported that the phosphorylation of Ser^{178} of Miz1 is required for its recruitment of HDAC1 to the target promoter (30). Consistently, here we showed that Ser^{178} phosphorylation is involved in the Miz1-mediated suppression of *Ifn* expression and viral clearance during IAV infection. Future investigation will identify the kinase(s) that phosphorylates Miz1 at Ser^{178} and thus reveal potential therapeutic targets.

The interplay between viruses and their hosts is of pivotal importance for determining the clinical outcome of infection (10–13). The host responds to viral infection by inducing an IFN response, which limits early viral spread and shapes adaptive immune responses. On the other hand, influenza viruses have developed multiple strategies to circumvent the first line of defense embodied by the IFN system to replicate efficiently and successfully establish an infection (23, 24). We found that IAV infection induced the accumulation of the Miz1 protein, which in turns repressed *Ifn* expression and promoted viral replication. We further showed that the cullin-E3 ligase family member CUL4B targeted Mule, the E3 ubiquitin ligase for Miz1, for ubiquitylation and degradation, resulting in the accumulation of Miz1, which appears to be a pro-viral host factor to promote viral propagation.

The cullin-E3 ligase family proteins are molecular scaffolds that have crucial roles in the posttranslational modification of cellular proteins involving ubiquitin (50, 51). Interestingly, it has been reported that several viruses, including human parainfluenza virus, hijack the cullin-E3 ligase family member CUL4B to target and degrade cellular proteins involved in host defense, which generates an amenable cellular environment for viral propagation (50–52). Our data show that CUL4B targets and degrades Mule, and thereby stabilizes Miz1 and inhibits *Ifn* expression during IAV infection. Thus, our study adds another layer to the pro-viral mechanism of CUL4B. Consistently, a CUL4B inhibitor represses viral replication in vitro and in vivo (53).

The role of the E3 ligase Mule in the host response against influenza virus infection has not been previously reported. Our data show that IAV infection induced the accumulation of Miz1 protein, which correlated with reduced Mule protein abundance. Silencing of Mule resulted in decreased IFN-β production in response to IAV infection, which was rescued by the simultaneous silencing of Miz1. These data suggest that Mule positively regulates antiviral innate immunity through the degradation of Miz1. In summary, our study demonstrates that Miz1 inhibits the antiviral innate immune response through epigenetic repression of *Ifn* expression. Additionally, we revealed a potential mechanism for influenza virus to escape from the host's immune surveillance by increasing Miz1 abundance through the CUL4B-mediated ubiquitylation and degradation of the Miz1 E3 ligase Mule.

Materials and Methods

Mice

Miz1(POZ)$^{fl/fl}$ mice (8- to 12-weeks old, male) on the C57BL/6 background have been described previously (30). Animal care and all experiments were performed in compliance with institutional and US National Institutes of Health guidelines and were approved by the Northwestern University Animal Care and Use Committee and the University of Illinois at Chicago Animal Care Committee.

Viruses and reagents

The IAV H1N1 strain A/WSN/33 (WSN) was propagated by allantoic inoculation of 10-day embryonated chicken eggs. Viral titers were determined as plaque-forming unit (PFUs) on Madin Darby canine kidney (MDCK) cell monolayers. MG-132 (#M8699, Sigma); MLN4924 (#HY-70062, MCE); poly(I:C) (#tlrl-piclv, Invivogen); lipofectamine2000 (#11668, Invitrogen); turbofect (R0531, Thermo Scientific); anti–β-actin (AC-15, Sigma); anti-Miz1 (H-190, Santa Cruz) for Western blotting, anti-Miz1 [(B-10X), sc-136985 Santa Cruz] for ChIP; anti-RelA (H-11, Santa Cruz) for ChIP; anti–p-JNK (#9255, Cell Signaling Technology); anti-JNK (#9252, Cell Signaling Technology); anti–p-ERK (#3179, Cell Signaling Technology); anti-ERK (#4695, Cell Signaling Technology); anti–p-p38 (#4511, Cell Signaling Technology); anti-p38 (#9790, Cell Signaling Technology); anti–p-IRF3 (#29047. Cell Signaling Technology); anti-IRF3 (#4302, Cell Signaling Technology) for Western blotting; anti-IRF3 (sc-376455, Santa Cruz) for ChIP; anti–p-IRF7 (#24129, Cell Signaling Technology); anti-IRF7 (#4920S, Cell Signaling Technology); anti-AcH3 (#8173, Cell Signaling Technology); anti-Histone H3 (#4620, Cell Signaling Technology); anti-HDAC1 (#10197–1-AP, Proteintech); anti-Mule (#4213, ProSci); anti-CUL4 (sc-377188, Santa Cruz) for Western blotting; anti-CUL4B (ab227724, Abcam) for coimmunoprecipitation, anti-M2-Flag (#F3165, Sigma); anti-Lamin B1 (12987–1-AP, Proteintech); anti–α-Tubulin (11224–1-AP, Proteintech); Plasmid encoding HA-Ub (WT) was kindly provided by J. Z. Chen (University of Texas Southwestern, Dallas, TX). The siRNA oligonucleotides specific SMART pool for CUL4B was from Dharmacon; siRNA oligonucleotides specific for Miz1, Mule and HDAC1 were listed in Table S1. The siMiz1(*Homo sapiens*) was purchased from Genepharma (Suzhou, China). Lentiviral shRNAs targeting human Miz1 (V3SVHS02_8619648, V3SVHS02_4756503, V3SVHS02_10078083; Horizon Discovery) or non-targeting control (Cat # S02–005000-01;

Horizon Discovery). Lentiviral shRNAs targeting human Mule (V3SVHS09_5138611, V3SVHS09_6205369; Horizon Discovery).

Cell lines

HEK293 cells (CRL-1573; ATCC), A549 cells (CCL-185; ATCC), and BEAS-2B cells (95102433; Sigma) were cultured in RPMI 1640 medium supplemented with 10% fetal bovine serum (FBS), L-glutamine, and penicillin/streptomycin (P/S).

Viral infections

MLE12 cells were seeded into 6-well plates (5×10^5 cells per well) and cultured overnight. Cells were washed twice with phosphate-buffered saline (PBS) and infected with IAV A/WSN/33 in serum-free medium for 1 hours. Cells were then cultured for the times in the figure legends and harvested for Western blotting and qPCR analyses. Supernatants were collected for viral titer tests or ELISAs. For mouse infections, age- and gender-matched (8- to 10-week old) male Miz1(POZ)$^{fl/fl}$ mice were intratracheally instilled with Ad-null or Ad-Cre. Thirty days later, the mice were infected with IAV (2 PFU per mouse in 50 μl of PBS), and monitored for lethality for up to 14 days. In other experiments, on day 4 after viral infection, the lungs and BAL fluid were harvested for cytokine analysis by ELISA. In a separate group of mice, lung tissues were homogenized to determine viral titers with MDCK cells, as well as the expression of cytokine-encoding genes by q-PCR analysis.

Ubiquitylation assay

HEK293 cells (2×10^6/ml) were transfected with constructs encoding M2 (Flag)-tagged Mule or control vector and HA-tagged ubiquitin. Twenty-four hours later, the cells were treated with 20 μM MG132 for 2 hours and then infected with IAV A/WSN/33 (at an MOI of 3) for the times indicated in the figure legends. Cells were harvested in 150 μl of M2 buffer [20 mM Tris (pH 7.6), 250 mM NaCl, 3 mM EDTA, 3 mM EGTA, 0.5% Nonidet P-40, 1 mM DTT, 1 μg/ml aprotinin, 10 mM p-nitrophenyl phosphate (PNPP), and 1 mM Na_3VO_4] supplemented with 0.8 mM N-ethylmaleimide (NEM) and 5 μM ubiquitin aldehyde, followed by the addition of sodium dodecyl sulfate (SDS) to a final concentration of 1% and boiled for 5 min (to disrupt any intermolecular noncovalent bonds between proteins). Cell extracts were subjected to immunoprecipitation with anti-M2 (Flag) antibody, which was followed by Western blotting analysis with anti-HA antibody to detect HA-tagged ubiquitin.

Real-time quantitative RT-PCR (RT-qPCR)

Total RNA was isolated with TRIzol (Thermo Fisher Scientific) and subjected to cDNA synthesis with RNase H-reverse transcriptase (Invitrogen) and oligo (dT) primers. qPCR was performed with the SYBR Green Supermix (Bio-Rad) with at least three technical replicates. The expression of individual genes was calculated by the ΔΔCT method normalized to the expression of the housekeeping genes *Hprt* or *GAPDH*. The gene-specific primers used for qPCR analysis are listed in table S2.

Multiplex analysis of cytokines and IgE ELISA

The concentrations of IFN-α and IFN-β in the BAL fluid were quantified by multiplex assays (eBioscience; IFN-β: EPX01B-26044–901; IFN-α: EPX01A-26027–901). The concentration of IFN-β in the culture medium 24 hours after infection with influenza A/WSN/33 virus (at an MOI of 1) or 48 hours after transfection with poly I:C (1 μg/ml) was detected by enzyme linked immunosorbent assay (ELISA) kit according to the manufacturer's instructions (CHE0084 and CHE0274, 4A Biotech Co .Ltd).

Dual-luciferase assay

Cells were transfected with *Ifnb1*-promoter luciferase reporter plasmid and a *Renilla* reporter construct at a ratio of 1:100 with lipofectamine 2000. Twenty-four hours after transfection, the cells were infected with Influenza A/WSN/33 (at an MOI of 3) for the times indicated in the figure legends. Cells were harvested, and the firefly luciferase and *Renilla* reporter activities were detected with a Dual-Glo Luciferase Assay System (E2920, Promega). Firefly luciferase activities were normalized to *Renilla* luminescence in each sample.

Plaque assays

MDCK cells were plated into a 6-well plate at a density of 1.5×10^6/well and cultured overnight until the cells formed a confluent monolayer. The culture medium was aspirated, and the cells were washed twice with PBS. The viruses were diluted in DMEM containing 1% BSA and added into the cells (1 ml/well). Cells were then incubated at 37°C for 1hour, and the cell culture plates were gently shaken every 15 min. One hour after the incubation, the cell culture medium was aspirated and the cells were washed twice with PBS, followed by the addition of the maintenance medium specific for plaque assays [2×DMEM (containing 1% BSA) mixed with 2.4% avicel (dissolved in distilled water) at 1:1 ratio, with N-acetyl trypsin (1.5 ng/ml)]. Cells were continually incubated at 37°C for 48 hours. The cell culture medium was removed, and the cells were washed with PBS, followed by the addition of 2 ml of black-blue staining solution (1 g of Naphthalene black, 60 ml of glacial acetic acid, 13.6 g anhydrous sodium acetate, and 1 L of distilled H_2O) into each well at room temperature for 10 min.

Chromatin immunoprecipitation (ChIP) assays

Cells were treated with 25 mM EGS for 20 min and then fixed with 1% formaldehyde for 10 min. 1 M glycine (dissolved in PBS) was used to quench the fixation. Cells were then lysed with ChIP SDS Lysis Buffer (Millipore, Catalog # 20–163) with protease inhibitors (100 mM PMSF, 10 mM PNPP, 1 mM Na_3VO_4, 1 mM DTT, 1 μg/ml aprotinin). Lysates were subjected to sonication on ice to shear DNA to fragments between 200 and 500 bp in size. Sonication efficiency was determined by analyzing samples by 1% agarose gel electrophoresis. Sonicated DAN (50 μg) was subjected to immunoprecipitation with the appropriate antibody (1 to 2 μg). Precipitated DNA-bead complexes were washed once with Low Salt Immune Complex Wash Buffer (Catalog # 20–154), once with High Salt Immune Complex Wash Buffer (Catalog # 20–155), and twice each with LiCl Immune Complex Wash Buffer (Catalog # 20–156) and TE Buffer (Catalog # 20–157). Eluted DNA was

purified and subjected to qPCR with primers corresponding to the PRDIII-II region of the *Ifnb1* promoter (table S2) (54). qPCR values from ChIP DNA were normalized to input DNA. For histone modification analyses, DNA bound by acetylated histone 3 (AcH3) was normalized to total Histone-3 (H3)–bound DNA.

Cell fractionation assay

Cytoplasmic and nuclear extracts were prepared with the Beyotime Nuclear and Cytoplasmic Extraction Reagents from Beyotime Inc. (Nantong, Jiangsu, China). After 24 hours of infection with influenza A/WSN/33 infection (at an MOI of 1), the procedure was conducted according to the manufacturer's instructions. The proteins were quantitated with a BCA protein assay kit and subsequently analyzed by Western blotting.

Statistical analysis

Data were analyzed by an unpaired Student's *t*-test with the assumption of a normal distribution of data and equal sample variance. Sample sizes were selected based on preliminary results to ensure an adequate power. Mice were randomly assigned to groups, and data were collected in a blinded manner. All data were included for analysis. Significance was considered at $P < 0.05$, and P values are described as follows: ns, $P > 0.05$; $*P < 0.05$; $**P < 0.01$; $***P < 0.001$. The N number represents biological replicates. Independent experiments were performed at least three times.

Supplementary Material

Refer to Web version on PubMed Central for supplementary material.

Acknowledgments:

We thank S.-C. Sun (University of Texas MD Anderson Cancer Center) for kindly providing the ifnb-1-promoter luciferase reporter construct. We thank Z. J. Chen (University of Texas Southwestern, Dallas, TX) for providing the plasmid encoding HA-Ub (WT).

Funding:

J.L. is supported by the US National Institutes of Health (HL141459). S.L. is supported by the National Natural Science Foundation of China (81728007), major scientific and technological projects of Guangdong Province (2019B020202002), and evidence-based capacity building project of Traditional Chinese Medicine (2019XZZX-LG04). W.W. is supported by funding from the Guangzhou Science and Technology Project (2023A03J0287).

References and Notes

1. Krammer F, Smith GJD, Fouchier RAM, Peiris M, Kedzierska K, Doherty PC, et al. Influenza. Nat Rev Dis Primers. 2018;4(1):3. [PubMed: 29955068]
2. Murphy SL, Xu J, Kochanek KD. Deaths: final data for 2010. National vital statistics reports : from the Centers for Disease Control and Prevention, National Center for Health Statistics, National Vital Statistics System. 2013;61(4):1–117.
3. Kumar B, Asha K, Khanna M, Ronsard L, Meseko CA, Sanicas M. The emerging influenza virus threat: status and new prospects for its therapy and control. Archives of virology. 2018;163(4):831–44. [PubMed: 29322273]
4. Xue KS, Moncla LH, Bedford T, Bloom JD. Within-Host Evolution of Human Influenza Virus. Trends in microbiology. 2018;26(9):781–93. [PubMed: 29534854]

5. Treanor J Influenza vaccine--outmaneuvering antigenic shift and drift. The New England journal of medicine. 2004;350(3):218–20. [PubMed: 14724300]
6. Krammer F, Palese P. Advances in the development of influenza virus vaccines. Nat Rev Drug Discov. 2015;14(3):167–82. [PubMed: 25722244]
7. Eisfeld AJ, Neumann G, Kawaoka Y. At the centre: influenza A virus ribonucleoproteins. Nat Rev Microbiol. 2015;13(1):28–41. [PubMed: 25417656]
8. Denney L, Ho LP. The role of respiratory epithelium in host defence against influenza virus infection. Biomed J. 2018;41(4):218–33. [PubMed: 30348265]
9. Whitsett JA, Alenghat T. Respiratory epithelial cells orchestrate pulmonary innate immunity. Nat Immunol. 2015;16(1):27–35. [PubMed: 25521682]
10. Kawai T, Akira S. Innate immune recognition of viral infection. Nat Immunol. 2006;7(2):131–7. [PubMed: 16424890]
11. Goubau D, Deddouche S, Reis e Sousa C. Cytosolic sensing of viruses. Immunity. 2013;38(5):855–69. [PubMed: 23706667]
12. Iwasaki A, Pillai PS. Innate immunity to influenza virus infection. Nat Rev Immunol. 2014;14(5):315–28. [PubMed: 24762827]
13. De Giovanni M, Cutillo V, Giladi A, Sala E, Maganuco CG, Medaglia C, et al. Spatiotemporal regulation of type I interferon expression determines the antiviral polarization of CD4+ T cells. Nature Immunology. 2020;21(3):321–30. [PubMed: 32066949]
14. McNab F, Mayer-Barber K, Sher A, Wack A, O'Garra A. Type I interferons in infectious disease. Nat Rev Immunol. 2015;15(2):87–103. [PubMed: 25614319]
15. Ivashkiv LB, Donlin LT. Regulation of type I interferon responses. Nat Rev Immunol. 2014;14(1):36–49. [PubMed: 24362405]
16. Kilian M The oral microbiome - friend or foe? European journal of oral sciences. 2018;126 Suppl 1:5–12. [PubMed: 30178561]
17. Rouse BT, Sehrawat S. Immunity and immunopathology to viruses: what decides the outcome? Nat Rev Immunol. 2010;10(7):514–26. [PubMed: 20577268]
18. Fitzgerald KA, McWhirter SM, Faia KL, Rowe DC, Latz E, Golenbock DT, et al. IKKepsilon and TBK1 are essential components of the IRF3 signaling pathway. Nat Immunol. 2003;4(5):491–6. [PubMed: 12692549]
19. Sharma S, tenOever BR, Grandvaux N, Zhou GP, Lin R, Hiscott J. Triggering the interferon antiviral response through an IKK-related pathway. Science. 2003;300(5622):1148–51. [PubMed: 12702806]
20. Honda K, Takaoka A, Taniguchi T. Type I interferon [corrected] gene induction by the interferon regulatory factor family of transcription factors. Immunity. 2006;25(3):349–60. [PubMed: 16979567]
21. Panne D, Maniatis T, Harrison SC. An atomic model of the interferon-beta enhanceosome. Cell. 2007;129(6):1111–23. [PubMed: 17574024]
22. Wang J, Basagoudanavar SH, Wang X, Hopewell E, Albrecht R, García-Sastre A, et al. NF-kappa B RelA subunit is crucial for early IFN-beta expression and resistance to RNA virus replication. J Immunol. 2010;185(3):1720–9. [PubMed: 20610653]
23. Katze MG, He Y, Gale M, Jr. Viruses and interferon: a fight for supremacy. Nat Rev Immunol. 2002;2(9):675–87. [PubMed: 12209136]
24. Haller O, Kochs G, Weber F. The interferon response circuit: induction and suppression by pathogenic viruses. Virology. 2006;344(1):119–30. [PubMed: 16364743]
25. Wanzel M, Herold S, Eilers M. Transcriptional repression by Myc. Trends Cell Biol. 2003;13(3):146–50. [PubMed: 12628347]
26. Peukert K, Staller P, Schneider A, Carmichael G, Hänel F, Eilers M. An alternative pathway for gene regulation by Myc. Embo j. 1997;16(18):5672–86. [PubMed: 9312026]
27. Herold S, Wanzel M, Beuger V, Frohme C, Beul D, Hillukkala T, et al. Negative regulation of the mammalian UV response by Myc through association with Miz-1. Mol Cell. 2002;10(3):509–21. [PubMed: 12408820]

28. Saito M, Novak U, Piovan E, Basso K, Sumazin P, Schneider C, et al. BCL6 suppression of BCL2 via Miz1 and its disruption in diffuse large B cell lymphoma. Proceedings of the National Academy of Sciences of the United States of America. 2009;106(27):11294–9. [PubMed: 19549844]
29. Si J, Yu X, Zhang Y, DeWille JW. Myc interacts with Max and Miz1 to repress C/EBPdelta promoter activity and gene expression. Molecular cancer. 2010;9:92. [PubMed: 20426839]
30. Do-Umehara HC, Chen C, Urich D, Zhou L, Qiu J, Jang S, et al. Suppression of inflammation and acute lung injury by Miz1 via repression of C/EBP-delta. Nature immunology. 2013;14(5):461–9. [PubMed: 23525087]
31. Zinn K, DiMaio D, Maniatis T. Identification of two distinct regulatory regions adjacent to the human beta-interferon gene. Cell. 1983;34(3):865–79. [PubMed: 6313211]
32. Ludwig S, Ehrhardt C, Neumeier ER, Kracht M, Rapp UR, Pleschka S. Influenza virus-induced AP-1-dependent gene expression requires activation of the JNK signaling pathway. The Journal of biological chemistry. 2001;276(24):10990–8.
33. Kujime K, Hashimoto S, Gon Y, Shimizu K, Horie T. p38 mitogen-activated protein kinase and c-jun-NH2-terminal kinase regulate RANTES production by influenza virus-infected human bronchial epithelial cells. Journal of immunology (Baltimore, Md : 1950). 2000;164(6):3222–8. [PubMed: 10706714]
34. Mori I, Goshima F, Koshizuka T, Koide N, Sugiyama T, Yoshida T, et al. Differential activation of the c-Jun N-terminal kinase/stress-activated protein kinase and p38 mitogen-activated protein kinase signal transduction pathways in the mouse brain upon infection with neurovirulent influenza A virus. The Journal of general virology. 2003;84(Pt 9):2401–8. [PubMed: 12917461]
35. Jin J, Hu H, Li HS, Yu J, Xiao Y, Brittain GC, et al. Noncanonical NF-κB pathway controls the production of type I interferons in antiviral innate immunity. Immunity. 2014;40(3):342–54. [PubMed: 24656046]
36. Tessarz P, Kouzarides T. Histone core modifications regulating nucleosome structure and dynamics. Nat Rev Mol Cell Biol. 2014;15(11):703–8. [PubMed: 25315270]
37. Strahl BD, Allis CD. The language of covalent histone modifications. Nature. 2000;403(6765):41–5. [PubMed: 10638745]
38. Sterner DE, Berger SL. Acetylation of histones and transcription-related factors. Microbiol Mol Biol Rev. 2000;64(2):435–59. [PubMed: 10839822]
39. Yang XJ, Seto E. HATs and HDACs: from structure, function and regulation to novel strategies for therapy and prevention. Oncogene. 2007;26(37):5310–8. [PubMed: 17694074]
40. Nusinzon I, Horvath CM. Positive and Negative Regulation of the Innate Antiviral Response and Beta Interferon Gene Expression by Deacetylation. Molecular and Cellular Biology. 2006;26(8):3106–13. [PubMed: 16581785]
41. Yang Y, Do H, Tian X, Zhang C, Liu X, Dada LA, et al. E3 ubiquitin ligase Mule ubiquitinates Miz1 and is required for TNFalpha-induced JNK activation. Proc Natl Acad Sci U S A. 2010;107(30):13444–9. [PubMed: 20624960]
42. Yi J, Lu G, Li L, Wang X, Cao L, Lin M, et al. DNA damage-induced activation of CUL4B targets HUWE1 for proteasomal degradation. Nucleic acids research. 2015;43(9):4579–90. [PubMed: 25883150]
43. Liu F, Cao L, Zhang T, Chang F, Xu Y, Li Q, et al. CRL4B(RBBP7) targets HUWE1 for ubiquitination and proteasomal degradation. Biochemical and biophysical research communications. 2018;501(2):440–7. [PubMed: 29738775]
44. De Clercq E Antiviral agents active against influenza A viruses. Nat Rev Drug Discov. 2006;5(12):1015–25. [PubMed: 17139286]
45. Petrova VN, Russell CA. The evolution of seasonal influenza viruses. Nat Rev Microbiol. 2018;16(1):47–60. [PubMed: 29081496]
46. Gounder AP, Boon ACM. Influenza Pathogenesis: The Effect of Host Factors on Severity of Disease. J Immunol. 2019;202(2):341–50. [PubMed: 30617115]
47. Natoli G, Saccani S, Bosisio D, Marazzi I. Interactions of NF-κB with chromatin: the art of being at the right place at the right time. Nature Immunology. 2005;6(5):439–45. [PubMed: 15843800]

48. Calao M, Burny A, Quivy V, Dekoninck A, Van Lint C. A pervasive role of histone acetyltransferases and deacetylases in an NF-kappaB-signaling code. Trends Biochem Sci. 2008;33(7):339–49. [PubMed: 18585916]

49. Thanos D, Maniatis T. Identification of the rel family members required for virus induction of the human beta interferon gene. Mol Cell Biol. 1995;15(1):152–64. [PubMed: 7799921]

50. Jackson S, Xiong Y. CRL4s: the CUL4-RING E3 ubiquitin ligases. Trends Biochem Sci. 2009;34(11):562–70. [PubMed: 19818632]

51. Sarikas A, Hartmann T, Pan ZQ. The cullin protein family. Genome Biol. 2011;12(4):220. [PubMed: 21554755]

52. Li T, Chen X, Garbutt KC, Zhou P, Zheng N. Structure of DDB1 in complex with a paramyxovirus V protein: viral hijack of a propeller cluster in ubiquitin ligase. Cell. 2006;124(1):105–17. [PubMed: 16413485]

53. Sun H, Yao W, Wang K, Qian Y, Chen H, Jung YS. Inhibition of neddylation pathway represses influenza virus replication and pro-inflammatory responses. Virology. 2018;514:230–9. [PubMed: 29248752]

54. Jin J, Hu H, Li HS, Yu J, Xiao Y, Brittain GC, et al. Noncanonical NF-κB pathway controls the production of type I interferons in antiviral innate immunity. Immunity. 2014;40(3):342–54. [PubMed: 24656046]

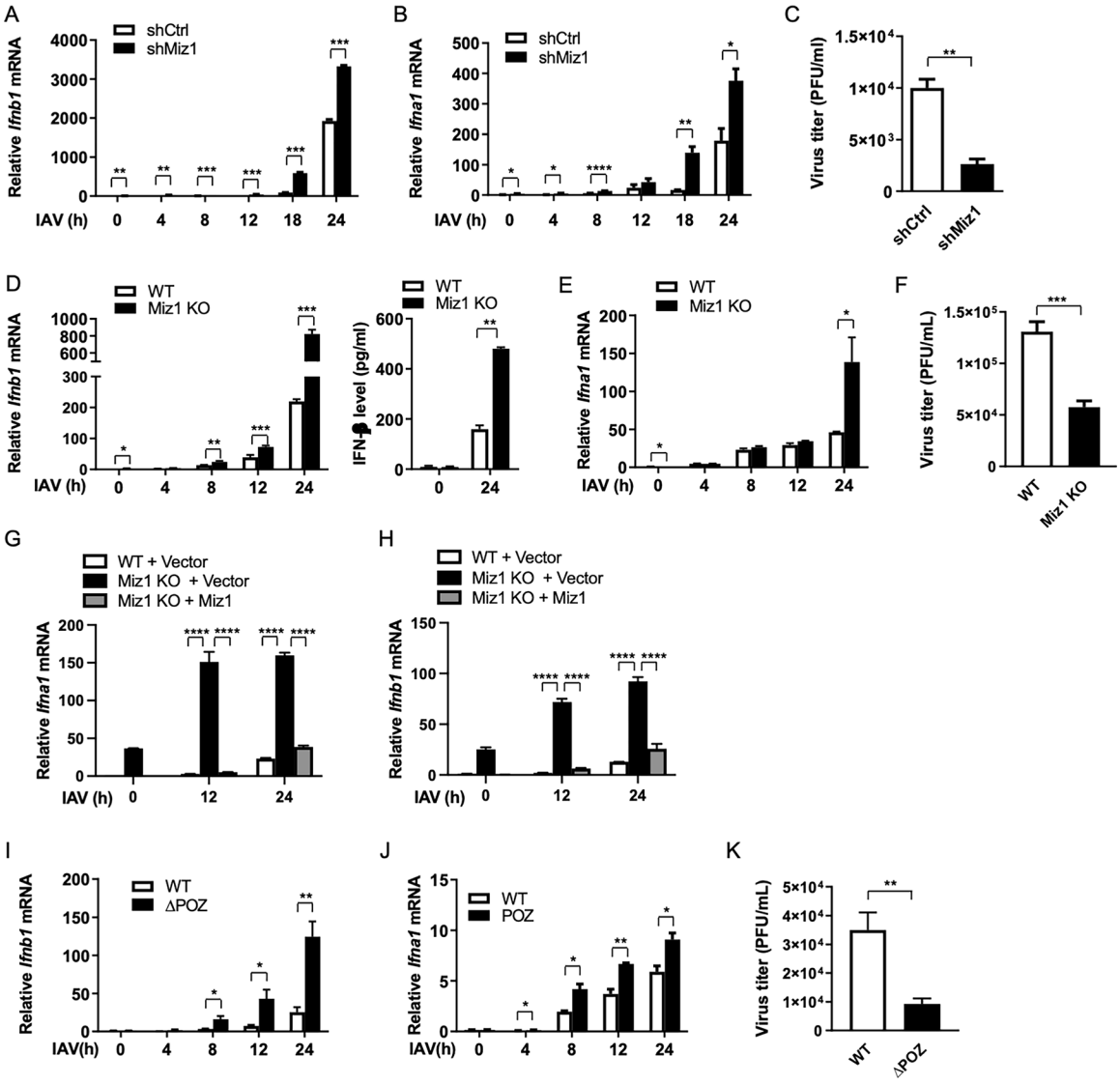

Fig. 1. Miz1 inhibits type I IFN expression and promotes viral replication during IAV infection of mouse lung epithelial cells.

(**A** to **K**) Analysis of the relative abundances of *Ifna1* and *Ifnb1* mRNAs, amounts of IFN-β secreted, and viral titers in WSN-infected MLE-12/shCtrl and MLE-12/shMiz1 cells (A to C), in control WT and MLE-12/Miz1 KO cells (D to F), in MLE-12/Miz1 KO cells supplemented with exogenous Miz1 (G and H), and in MLE12–Miz1(WT) and MLE-12–Miz1(ΔPOZ) cells (I to K). Data are means ± SEM of three experiments. *$P < 0.05$; **$P < 0.01$; ***$P < 0.001$; ****$P < 0.0001$.

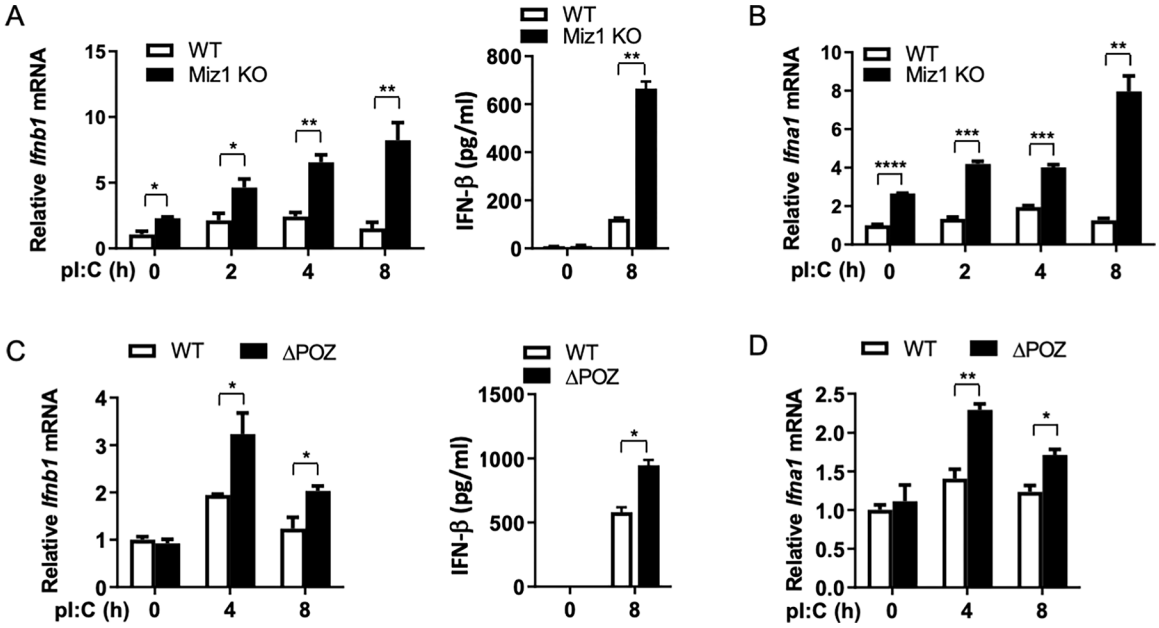

Fig. 2. Miz1 inhibits poly(I:C)-induced type I IFN expression in mouse lung epithelial cells.

mRNA (**A** to **D**) Analysis of the relative expression of *Ifna1* and *Ifnb1* mRNAs (A to D) and the amounts of IFN-β secreted (A and C) by poly(I:C)-treated control WT and MLE-12/Miz1 KO cells (A and B) and in MLE12–Miz1(WT) and MLE-12–Miz1(ΔPOZ) cells (C and D) at the indicated times. Data are means ± SEM of three experiments. *$P < 0.05$; **$P < 0.01$; ***$P < 0.001$.

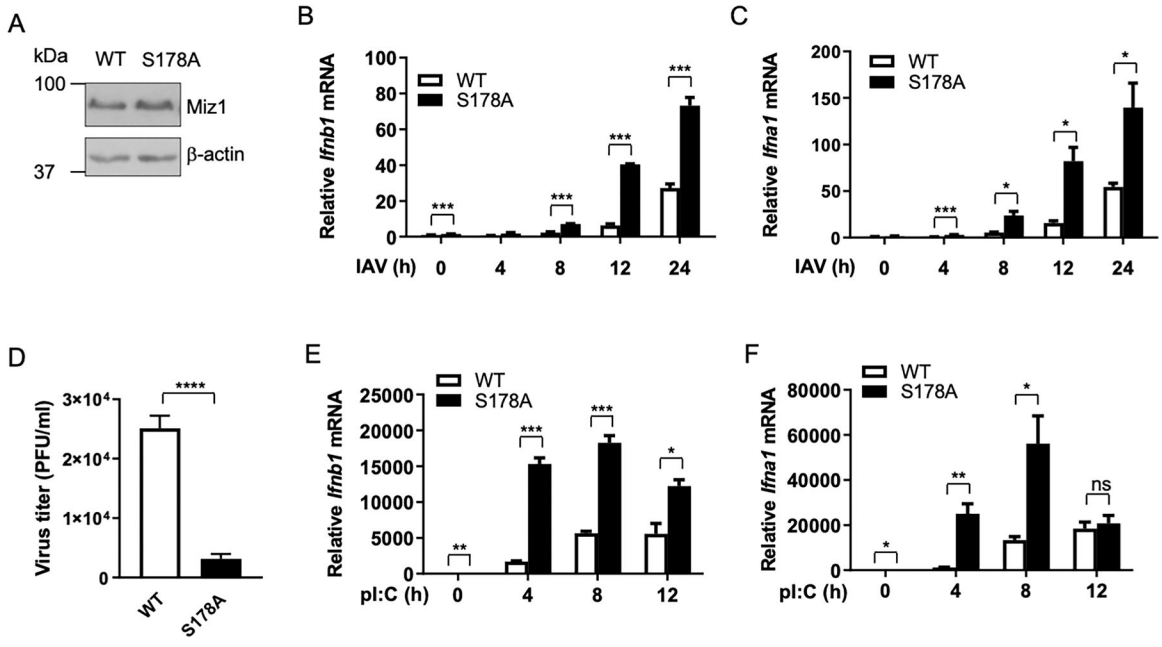

Fig. 3. Miz1-mediated suppression of type I IFN expression and viral clearance depends on the phosphorylation of Miz1 at Ser^{178}.

(**A**) Western blotting analysis of Miz1 protein (WT or S178A) in MLE-12/Miz1(WT) or MLE-12/Miz1(S178A) cells. Data are representative of three experiments. (**B** to **D**) Analysis of the relative amounts of *Ifna1* and *Ifnb1* mRNAs (A and B) and viral titers in WSN-infected MLE-12/Miz1(WT) and MLE-12/Miz1(S178A) cells. (**E** and **F**) Analysis of the relative amounts of *Ifna1* and *Ifnb1* mRNAs in poly(I:C)-treated MLE-12/Miz1(WT) and MLE-12/Miz1(S178A) cells. Data are means ± SEM of three experiments. *$P < 0.05$; **$P < 0.01$; ***$P < 0.001$; ****$P < 0.0001$; ns, not significant.

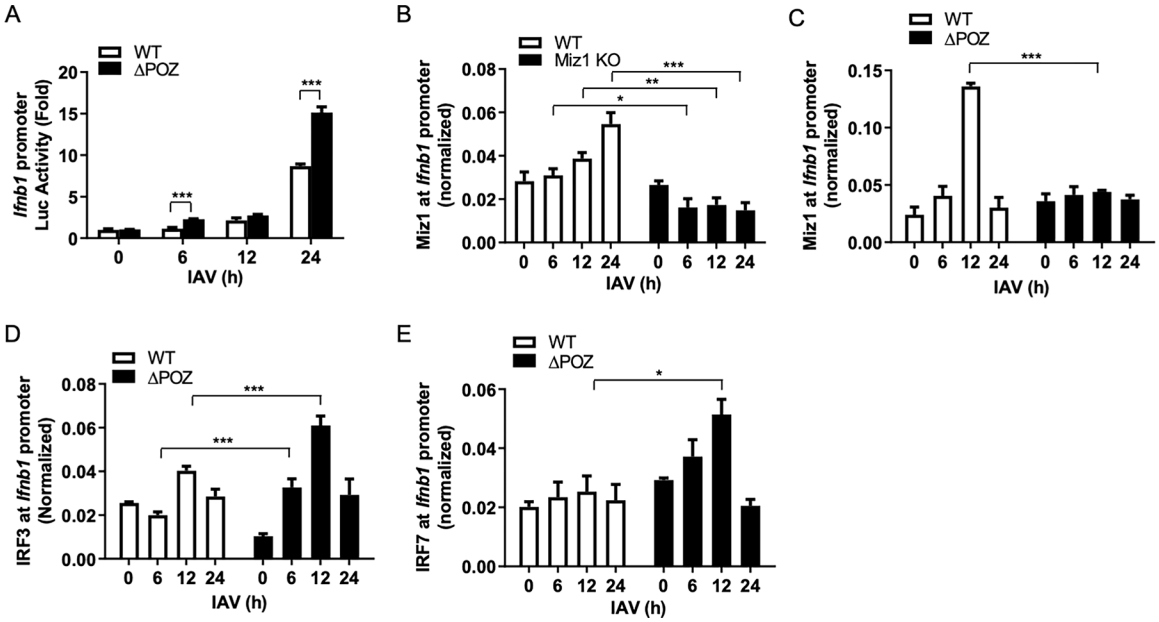

Fig. 4. Miz1 interferes with the binding of IRF3 and IRF7 to the *Ifnb1* promoter.

(**A**) Analysis of *Ifnb1* promoter activity (normalized to the *Renilla* luminescence of the internal transfection control) in WSN-infected MLE12–Miz1(WT) and MLE-12–Miz1(ΔPOZ) cells. (**B** and **C**) ChIP analysis of the recruitment of Miz1 to the *Ifnb1* promoter in WSN-infected control WT and MLE-12/Miz1 KO cells (B) and in MLE12–Miz1(WT) and MLE-12–Miz1(ΔPOZ) cells (C). (**D** and **E**) ChIP analysis of the recruitment of IRF3 (D) and IRF7 (E) to the *Ifnb1* promoter in WSN-infected MLE12–Miz1(WT) and MLE-12–Miz1(ΔPOZ) cells. Data are means ± SEM of three experiments. *$P < 0.05$; **$P < 0.01$; ***$P < 0.001$; ****$P < 0.0001$.

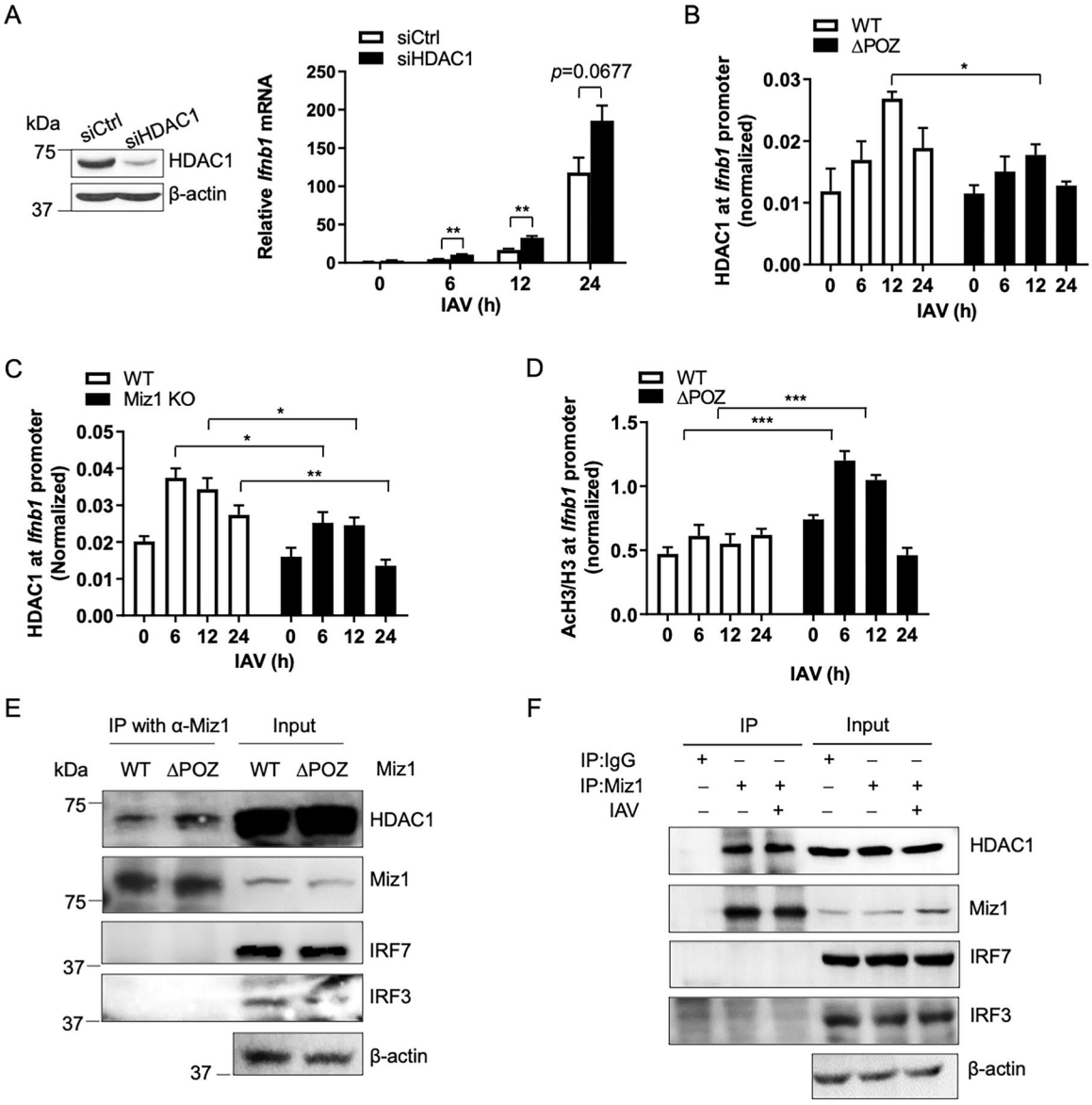

Fig. 5. Miz1 recruits HDAC1 to the *Ifnb1* promoter.

(**A**) Left: Western blotting analysis of HDAC1 protein in MLE-12 cells treated with control siRNA (siCtrl) or siRNA for HDAC1-specific siRNA (siHDAC1). Right: Analysis of the relative abundance of *Ifnb1* mRNA in WSN-infected MLE-12 cells pretreated with the indicated siRNAs. (**B** and **C**) ChIP analysis of the recruitment of HDAC1 to the *Ifnb1* promoter in WSN-infected MLE12–Miz1(WT) and MLE-12–Miz1(ΔPOZ) cells (B) and in control WT and MLE-12/Miz1 KO cells (C). (**D**) ChIP analysis of the enrichment of acetyl histone H3 (acetylated lysines 9 and 14, normalized to total histone H3 abundance) on the *Ifnb1* promoter in WSN-treated MLE12–Miz1(WT) and MLE-12–Miz1(ΔPOZ) cells. Data are means ± SEM of three experiments. $*P < 0.05$; $**P < 0.01$; $***P < 0.001$. (**E** and **F**) Western blotting analysis of the co-immunoprecipitation of endogenous Miz1 and HDAC1 under resting conditions (E) or in response to WSN infection (F) in MLE12–Miz1(WT) and MLE-12–Miz1(ΔPOZ) cells. Blots are representative of three experiments.

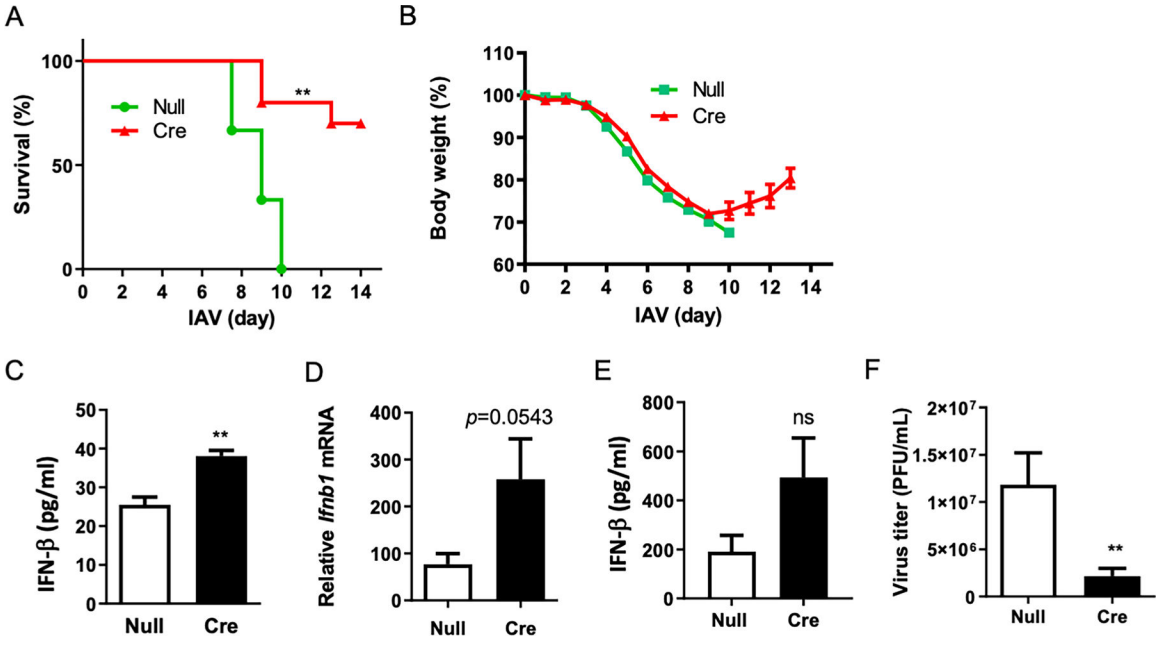

Fig. 6. Loss of function of Miz1 augments type I IFN expression and improves survival in IAV-infected mice.

(**A** and **B**) Survival rates (A) and body weight loss (B) of WSN-infected control Miz1(POZ)$^{fl/fl}$ and Miz1$^{\Delta POZ\text{-}lung}$ mice. Data are from 10 to 12 mice per genotype. (**C** to **E**) Quantification of the amounts of IFN-β in the BAL fluid (C and E) and of the relative amount of *Ifnb1* mRNA in whole-lung homogenates (D) of WSN-infected control Miz1(POZ)$^{fl/fl}$ and Miz1$^{\Delta POZ\text{-}lung}$ mice. Data are from six mice per genotype. (**F**) Viral titers in whole-lung homogenates from WSN-infected control Miz1(POZ)$^{fl/fl}$ and Miz1$^{\Delta POZ\text{-}lung}$ mice. Data are means ± SEM of six mice per genotype. $^{**}P < 0.01$; ns, not significant.

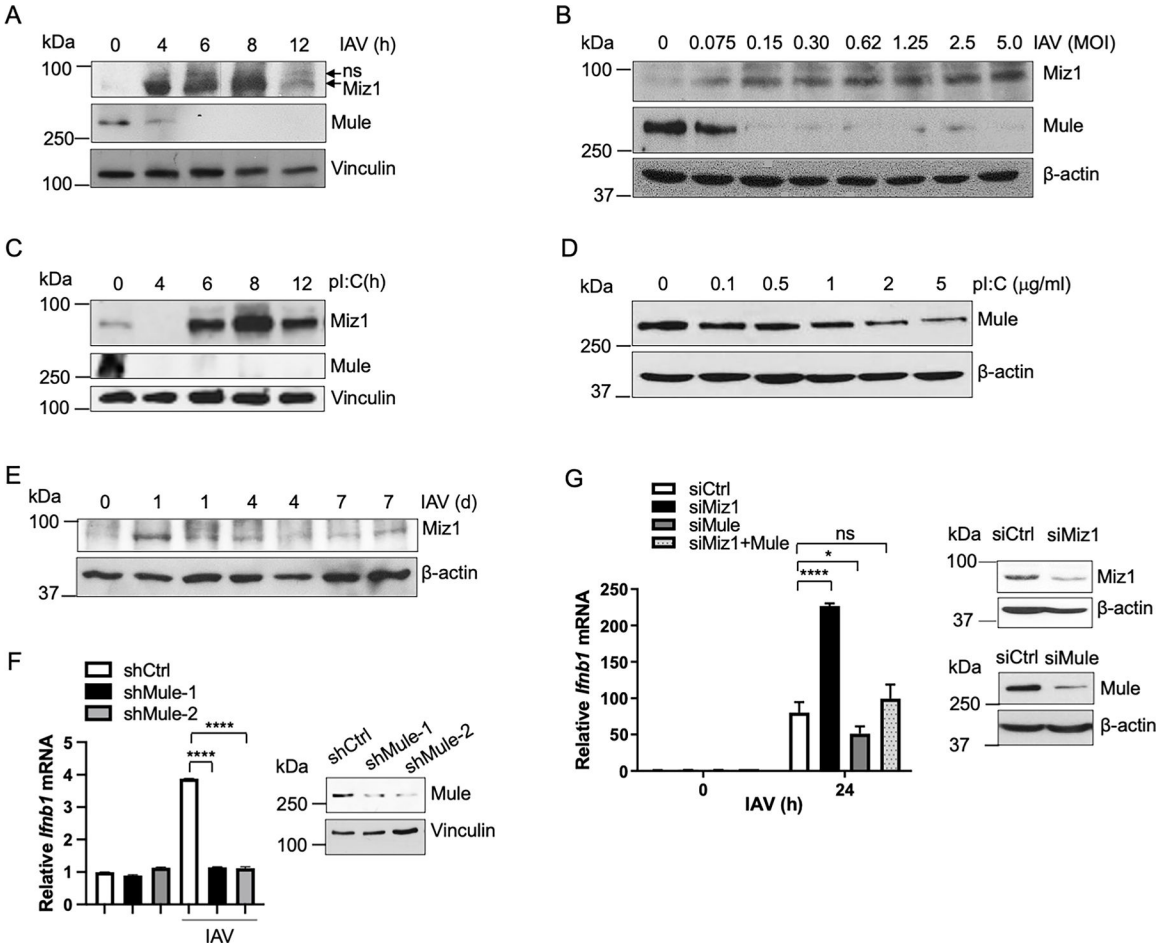

Fig. 7. IAV infection induces loss of the Miz1 E3 ubiquitin ligase Mule and accumulation of Miz1.

(**A** and **B**) Western blotting analysis of Miz1 and Mule in MLE-12 cells infected with WSN (at an MOI of 1) for the indicated times (A) and in MLE-12 cells infected with WSN at the indicated MOIs (B). Blots are representative of three experiments. (**C** and **D**) Western blotting analysis of Miz1 and Mule in MLE-12 cells that were treated with poly(I:C) for the indicated times (C) and in MLE-12 cells that were treated with the indicated concentrations of poly(I:C) for 8 hours (D). (**E**) Western blotting analysis of Miz1 protein in whole-lung homogenates of WT mice infected with WSN for the indicated times. (**F**) Analysis of the relative abundance of *Ifnb1* mRNA in WSN-infected MLE-12 cells stably expressing the indicated Mule-specific shRNAs. (**G**) Left: Analysis of the relative abundance of *Ifnb1* mRNA in WSN-infected MLE-12 cells pre-treated with the indicated siRNAs. Right: Western blotting analysis of Miz1 and Mule proteins in MLE-12 cells treated with the indicated siRNAs. Data are means ± SEM of three experiments. *$P < 0.05$; ****$P < 0.0001$; ns, not significant.

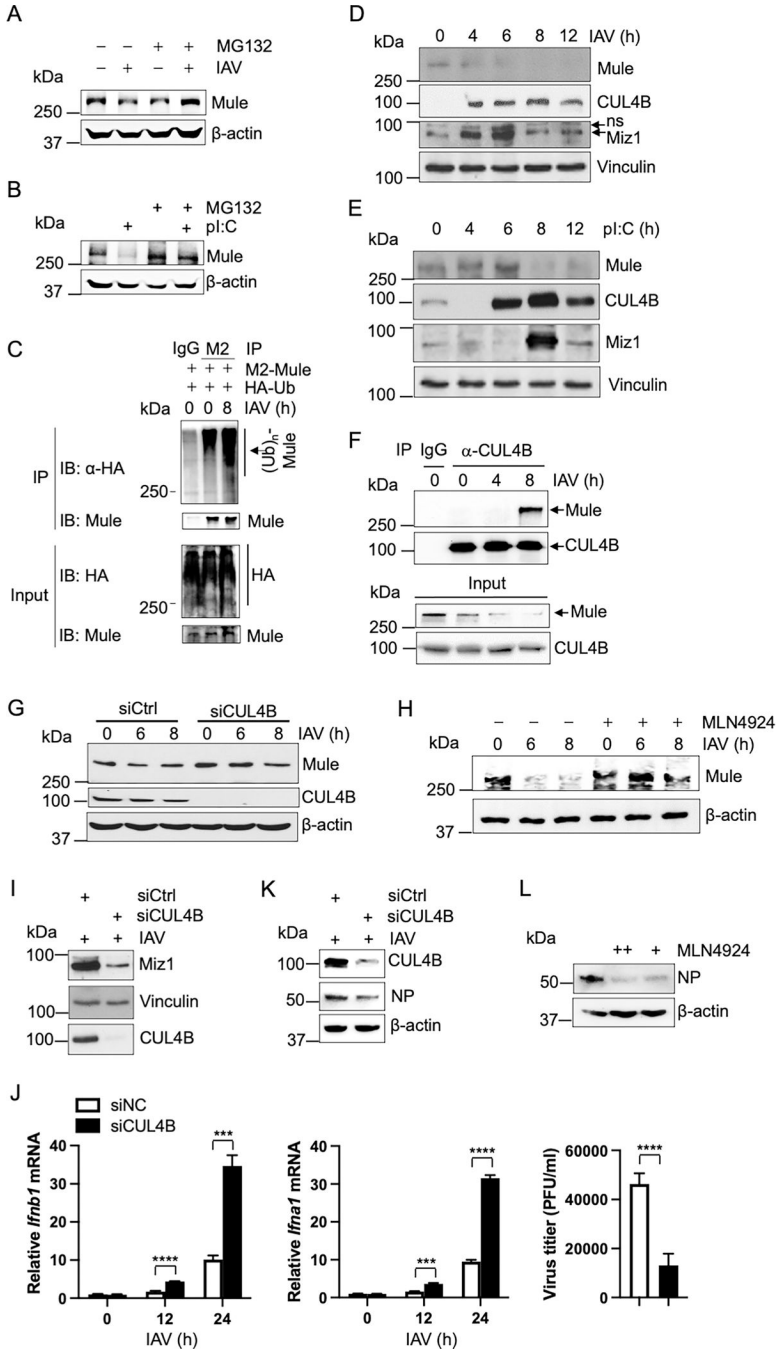

Fig. 8. IAV infection induces the production of CUL4B, which targets Mule for ubiquitylation and degradation.

(**A** and **B**) Western blotting analysis of Mule protein in MLE-12 cells that were infected with WSN at an MOI of 1 for 8 hours or were treated with poly(I:C) (1 μg/ml) for 8 hours in the absence or presence of 20 μM MG-132. Note thatMG-132 was added after WSN infection or poly(I:C) treatment. (**C**) HEK 293 cells were cotransfected with plasmids encoding M2-Mule and HA-Ub. Thirty-six hours later, the cells were infected with WSN. Ubiquitylation of M2-Mule was assessed by immunoprecipitation (IP) with anti-Flag (M2)

antibody in combination with Western blotting analysis with anti-HA antibody. (**D** and **E**) Western blotting analysis of CUL4B, Mule, and Miz1 in WSN-infected (D) and poly(I:C)-treated (E) MLE-12 cells. (**F**) Coimmunoprecipitation of endogenous Mule and CUL4B in WSN-infected MLE-12 cells. (**G** and **H**) Western blotting analysis of Mule in WSN-infected MLE-12 cells that were pretreated with the indicated siRNAs (G) or with 10 μM MLN4924 (a CUL4B inhibitor) (H). (**I** to **K**) Western blotting analysis of Miz1 protein (I), analysis of *Ifna* and *Ifnb* mRNA abundance and viral titers (J), and Western blotting analysis viral NP protein (K) in WSN-infected MLE-12 cells that were pretreated with control siRNA or CUL4B-specific siRNA. (**L**) Western blotting analysis of viral NP protein in WSN-infected MLE-12 cells that were pretreated with 10 μM (+) or 20 μM (++) MLN4924. Data are means ± SEM of three experiments. ***$P < 0.001$; ****$P < 0.0001$.

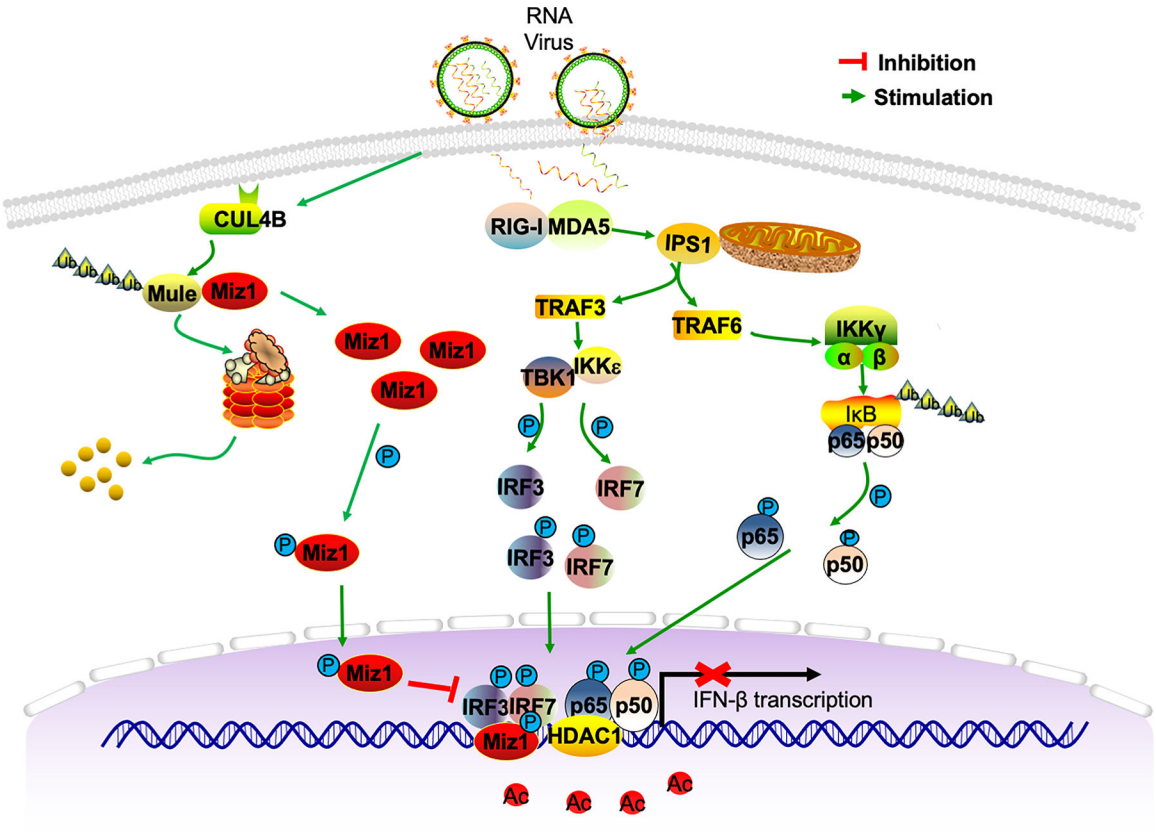

Fig. 9. Scheme for the IAV-induced accumulation of Miz1 and its repression of the type I IFN response.

Upon IAV infection, the IRF3, IRF7, and NF-κB signaling pathways are activated downstream of RIG-I, leading to induction of the expression of genes encoding type I IFNs. At the same time, the abundance of CUL4B is increased and it targets the Miz1 E3 ubiquitin ligase Mule for ubiquitylation and degradation. This leads to the accumulation of Miz1 protein, which in turn recruits HDAC1 to the *Ifnb1* promoter, resulting in histone deacetylation of the chromatin and interference in the binding of IRF3 and IRF7, thereby repressing *Ifnb1* expression and promoting viral replication.